CHEMISTRY
A EUROPEAN JOURNAL

DOI: 10.1002/chem.201102034

Multivalent Gold Glycoclusters: High Affinity Molecular Recognition by Bacterial Lectin PA-IL

Michael Reynolds,[a, b] Marco Marradi,[c, d] Anne Imberty,[a] Soledad Penadés,[c, d] and Serge Pérez*[a, b]

Abstract: Multivalent protein-carbohydrate interactions are involved in the initial stages of many fundamental biological and pathological processes through lectin–carbohydrate binding. The design of high affinity ligands is therefore necessary to study, inhibit and control the processes governed through carbohydrate recognition by their lectin receptors. Carbohydrate-functionalised gold nanoclusters (glyconanoparticles, GNPs) show promising potential as multivalent tools for studies in fundamental glycobiology research as well as biomedical applications. Here we present the synthesis and characterisation of galactose functionalised GNPs and their effectiveness as binding partners for PA-IL lectin from *Pseudomonas aeruginosa*. Interactions were evaluated by hemagglutination inhibition (HIA), surface plasmon resonance (SPR) and isothermal titration calorimetry (ITC) assays. Results show that the gold nanoparticle platform displays a significant cluster glycoside effect for presenting carbohydrate ligands with almost a 3000-fold increase in binding compared with a monovalent reference probe in free solution. The most effective GNP exhibited a dissociation constant (K_d) of 50 nM per monosaccharide, the most effective ligand of PA-IL measured to date; another demonstration of the potential of glyco-nanotechnology towards multivalent tools and potent anti-adhesives for the prevention of pathogen invasion. The influence of ligand presentation density on their recognition by protein receptors is also demonstrated.

Keywords: gold · lectin · multivalence · nanoparticle · protein–carbohydrate interactions

Introduction

Carbohydrates at the cell surface (glycolipids and glycoproteins) play key roles in the recognition mechanisms of cells and their external environment.[1] Specific, reversible interactions between these carbohydrates and protein receptors (lectins) are of great importance in many biological and pathological processes ranging from fertilisation and intercellular communication to bacterial invasion and tumour metastasis.[2] These lectin–carbohydrate interactions typically exhibit high specificity and weak affinities toward their carbohydrate ligand. In nature, this low affinity is compensated by the architecture of the lectin itself, containing typically two or more carbohydrate binding sites, and by the host presenting the carbohydrate ligands multivalently or as clusters on the cell surface.[3] The resulting interaction thus being a combination of several binding events, yet the overall binding is significantly greater than the combination of the individual binding events, that is, the "whole" of the interaction is greater than the sum of its parts. This effect is known as the multivalence or cluster–glycoside effect,[4–6] and is well documented for lectin–carbohydrate interactions for increasing ligand affinity and selectivity. Multivalence has been attributed to increasing structural complementarities between ligand and receptors,[3] as well as statistical effects such as effective concentrations and statistical rebinding.[7–12]

With this in mind, many multivalent "scaffolds" with various valencies and modes of ligand presentation have been developed. Synthetic oligosaccharides, themselves functionalised with suitable "spacer" molecules have been conjugated to a number of multivalent scaffolds ranging from cyclopeptides,[13,14] glycoproteins,[15–19] dendrimers and dendrons,[20–24] and polymers[25–27] to polymeric nanoparticles,[28,29] fullerenes,[30,31] calixarenes[32–35] and quantum dots.[36–40] Over the last decade, an integrated approach for the construction of a well-defined platform for presenting carbohydrates was developed. This strategy was based on the self-assembly of carbohydrate monolayers on the surface of gold particles, termed glyconanoparticles (GNPs).[41] Sev-

[a] Dr. M. Reynolds, Dr. A. Imberty, Dr. S. Pérez
CERMAV-CNRS, affiliated with the Université Joseph Fourier
BP 53, F-38041, Grenoble Cedex 9 (France)
Fax: (+33) 476-547-203
E-mail: serge.perez@cermav.cnrs.fr

[b] Dr. M. Reynolds, Dr. S. Pérez
European Synchrotron Radiation Facility
6 Rue Jules Horowitz, BP 220, 38043
Grenoble Cedex 9 (France)

[c] Dr. M. Marradi, Dr. S. Penadés
CIC biomaGUNE
PºMiramón 182, 20009 San Sebastian (Spain)

[d] Dr. M. Marradi, Dr. S. Penadés
Biomedical Research Networking Centre in Bioengineering
Biomaterials and Nanomedicine (CIBER-BBN)
PºMiramón 182, 20009 San Sebastian (Spain)

Supporting Information for this article is available on the WWW under http://dx.doi.org/10.1002/chem.201102034.

eral reviews have also been published on GNP synthesis, characterisation and application.[42–44] Functionalising nanoparticles with oligosaccharides has several advantages over other multivalent scaffolds: Their synthesis and functionalisation is a simple, one step process that allows the tuning of various physical properties (stability, water solubility, cytotoxic activity, particle core composition, etc.). Nanoparticle dimensions are comparable to biomacromolecules and can be adjusted by modifying particular experimental conditions. They are also globular in shape, making them ideal for providing a high valence glycocalyx-like surface for presenting oligosaccharide molecules. Furthermore, several molecules of interest can be attached to the same nanoparticle, giving rise to multifunctionality, and by altering the ratios of the molecules to be conjugated to the GNP surface, their presentation density can be controlled. Ligand presentation density has previously been shown to influence lectin-mediated recognition processes.[45–50] Finally, as well as their chemical and biochemical properties, nanoparticles of this size exhibit interesting physical properties due to quantum size effects, which could also be exploited in numerous applications.[51,52]

Due to their function, lectins are important targets for many analytical, diagnostic and therapeutic applications. Recently, our laboratory has characterised several bacterial lectins, which exhibit high affinities for monosaccharide ligands. In this report, the PA-IL (LecA) lectin from *Pseudomonas aeruginosa* is considered.[53] *P. aeruginosa* is an opportunistic bacteria responsible for numerous nosocomial infections in patients suffering from cystic fibrosis as well as the immunocompromised.[54,55] The virulence and host invasion of this bacterium is mediated by PA-IL and PA-IIL (LecB) lectins, which exhibit specificities for galactose and fucose, respectively. Therefore the design of high affinity ligands for these lectins is required as part of a combined approach for blocking lectin binding sites and inhibiting infection. This study presents galactose-functionalised GNPs for binding to PA-IL. Several GNPs were synthesised exhibiting varying galactose valencies and presentation densities and their binding properties studied by hemagglutination inhibition (HIA), surface plasmon resonance (SPR) and isothermal titration calorimetry (ITC) assays.

Results and Discussion

Synthesis: We have prepared and characterised a series of water-soluble gold GNPs functionalised with galactose, glucose and mannose neoglycoconjugates. The GNPs prepared exhibit varying presentation densities of the galactose and mannose ligands. The neoglycoconjugates synthesised and the GNPs prepared are summarised in Figure 1 and Table 1.

Synthesis of neoglycoconjugates 1–3: The thiol-functionalised neoglycoconjugate of glucose **1** was synthesised as previously reported.[56] The galactose neoglycoconjugate **2** was prepared as for its α-D-mannoside equivalent **3**,[56] and is shown in Scheme 1S (see the Supporting Information). In this study, the glucose neoglycoconjugate **1** has a short five-carbon linear aliphatic chain and acts as an inert ligand with respect to lectin interactions, allowing the modification of "active" galactoside/mannoside ligand presentation at the GNP surface. The galactose neoglycoconjugate **2** was conjugated to the GNP surface through the thiol-ending group of the amphiphilic linker as in previous studies.[56] This linker imparts good chemisorption to the GNP surface as well as

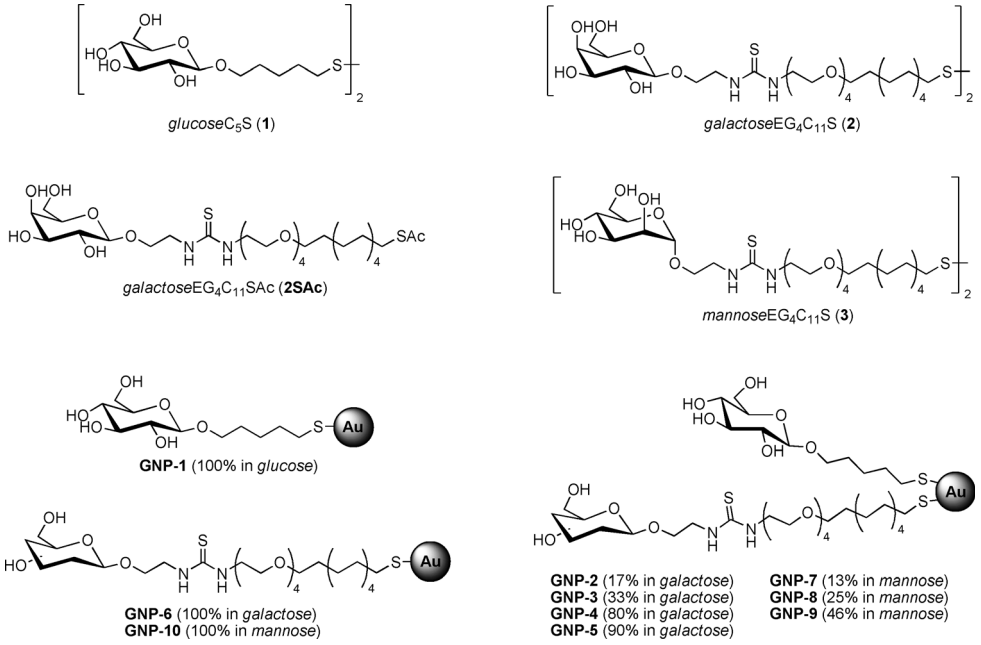

Figure 1. Ligands **1–3** synthesised for protecting Au clusters **GNP-1–GNP-10**. For clarity, the neoglycoconjugates **1**, **2** and **3** are named and depicted as disulfides.

Table 1. Summary of GNPs synthesised.

GNP	Average core diameter [nm]	Shell thickness [nm]	Average no. of Au atoms[a]	Average molecular formula	Average galactose valency	Average galactose valency [%]	Average M_w[a][kDa]
gluco							
GNP-1	(1.3±0.3)	0.8	100	$(C_{11}H_{21}O_6S)_{41}Au_{100}$	0	0	31.2
galacto/gluco							
GNP-2	(1.4±0.5)	1.9	120	$(C_{28}H_{55}N_2O_{10}S_2)_{12}(C_{11}H_{21}O_6S)_{59}Au_{120}$	12	17	47.9
GNP-3	(1.3±0.3)	2.2	79	$(C_{28}H_{55}N_2O_{10}S_2)_{15}(C_{11}H_{21}O_6S)_{30}Au_{79}$	15	33	33.6
GNP-4	(1.4±0.3)	2.6[b]	140	$(C_{28}H_{55}N_2O_{10}S_2)_{65}(C_{11}H_{21}O_6S)_{16}Au_{140}$	65	80	73.9
GNP-5	(1.4±0.3)	2.6[b]	100	$(C_{28}H_{55}N_2O_{10}S_2)_{57}(C_{11}H_{21}O_6S)_{7}Au_{100}$	57	90	58.3
GNP-6	(1.2±0.3)	2.6	70	$(C_{28}H_{55}N_2O_{10}S_2)_{67}Au_{70}$	67	100	56.9
manno/gluco					*manno* valency		
GNP-7	(1.5±0.4)	1.7	125	$(C_{28}H_{55}N_2O_{10}S_2)_{11}(C_{11}H_{21}O_6S)_{72}Au_{125}$	11 (Man)	13 (Man)	51.9
GNP-8	(1.7±0.4)	2.2	140	$(C_{28}H_{55}N_2O_{10}S_2)_{24}(C_{11}H_{21}O_6S)_{72}Au_{140}$	24 (Man)	25 (Man)	63.3
GNP-9	(1.6±0.4)	2.7	140	$(C_{28}H_{55}N_2O_{10}S_2)_{39}(C_{11}H_{21}O_6S)_{46}Au_{140}$	39 (Man)	46 (Man)	65.6
GNP-10	(1.2±0.3)	2.6	70	$(C_{28}H_{55}N_2O_{10}S_2)_{67}Au_{70}$	67 (Man)	100 (Man)	56.9

[a] The average number of gold atoms in the cluster, the molecular formulae, and the molecular weights were calculated according to the average gold core diameter by TEM and elemental analysis.[57] [b] Shell thickness extrapolated from GNP SAXS data.

ligand flexibility and aqueous solubility. The mannose neoglycoconjugate **3** and mannose-GNPs were used as negative controls to account for non-specific PA-IL-–GNP interactions.

Preparation of gold glyconanoparticles: The galactose- and mannose-protected glyconanoparticles (**GNP-6** and **GNP-10**) exhibit high ligand presentation densities for investigating lectin–carbohydrate interactions. **GNP-2**–**GNP-5** were prepared as hybrids of neoglycoconjugates **1** and **2** to study the influence of galactose presentation density on molecular recognition by PA-IL. Glucose **GNP-1** and mannose/glucose hybrids **GNP-7**–**GNP-10** were prepared as negative controls for the assays. All GNPs proved to be stable and soluble in aqueous environments.

All GNPs were prepared and characterised using procedures previously developed.[58,59] Briefly, a methanolic solution of the corresponding neoglycoconjugates was added to an aqueous solution of tetrachloroauric acid ($HAuCl_4$). In situ reduction of the resulting mixture with $NaBH_4$ gave a dark brown mixture, which was shaken for 2 h. The solvent was removed and the aggregates re-suspended in water. Exhaustive dialysis against water, followed by centrifugation and lyophilisation gave the GNPs as amorphous brown solids. They were characterised by ^{1}H NMR, FT-infrared spectroscopy, UV/Vis spectroscopy, elemental analysis, transmission electron microscopy (TEM) and small angle X-ray scattering (SAXS). The GNPs prepared are water-soluble, stable and can be treated as macromolecules. A summary of the GNPs produced can be found in Figure 1, Table 1 and in the Supporting Information.

The ^{1}H NMR spectra of the resulting GNPs featured broader peaks with regard to the neoglycoconjugates in free solution. From TEM, GNPs show an exceptionally small average core size (1.2–1.7 nm), with a uniform monomodal dispersion. Elemental analysis confirms for all GNPs the coverage density estimated by NMR. From GNP core size and elemental analysis, an average molecular formula was estimated according to previous work.[57] Due to the exceptionally small core size of the GNPs, surface plasmon resonance bands were not seen in the UV/Vis spectra. This is typical of AuNPs of core diameter <2 nm and has been observed for similar GNPs.[51,56] SAXS was used to confirm the size and size distribution of the core and, in combination with other techniques, give an estimate of the ligand shell radii in solution. The corresponding curves can be seen in the Supporting Information. Curves show scattered X-ray intensities due to particle shape, size and size distribution. Data were fitted with a spherical core-shell model with core radii and dispersion constrained to that measured by TEM.[60] Results from SAXS data will be discussed in detail in a separate paper. At low presentation densities of active ligands **2** or **3**, the organic shell thickness around the gold core is significantly thinner than the length of the active ligands in a linear conformation (by up to 50%). This suggests the active ligands fold and collapse on to the glucose shell perhaps to shield the hydrophobic gold core or form non-covalent contacts to other surface bound ligands. As active ligand density increases at the GNP surface, the ligands experience increasing steric effects from each other and are therefore encouraged to adopt a more linear display, perpendicular to the GNP surface (Figure 2, a more refined diagram can be found in the Supporting Information).

Usually GNPs are soluble in water and stable for several years in solution. However, some galactose containing

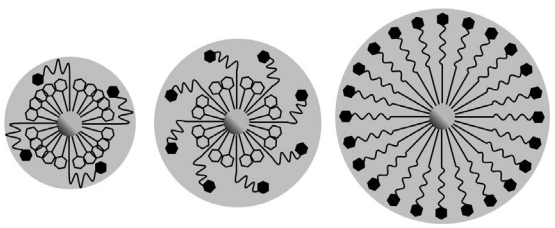

Figure 2. Schematic representation showing the variation of shell thickness with active ligand presentation density (1.8–2.2–2.6 nm for 10–25–100% respective presentation density). Solid hexagons represent active ligands, hollow hexagons represent inactive glucose ligands. Diagram not to scale.

GNPs studied here, although water-dispersible, were not soluble in sufficient quantity in buffer solutions such as **GNP-4** and **GNP-5**. ITC experiments involving these GNPs proved difficult.

Interaction studies: Binding inhibition by hemagglutination inhibition assay (HIA): Hybrid galactose-**GNP-2–6** were evaluated as ligands for PA-IL in a hemagglutination assay with rabbit erythrocytes. Glucose **GNP-1** and hybrid mannose-**GNP-8** were used as negative controls. Lectins are well known for their ability to agglutinate red blood cells. Measuring the minimum concentration of GNPs required to prevent this agglutination gives an indication of their average inhibition power. Hemagglutination assays were performed using PA-IL (5 $\mu g\,mL^{-1}$) with GNPs in serial dilutions varying from 2 $mg\,mL^{-1}$ to 1 $\mu g\,mL^{-1}$. Galactose (and mannose) concentrations on the GNPs were confirmed by a modified phenol–sulphuric acid method.[61] Looking at the photographs of the assay (see the Supporting Information, Figure 5S), a yellow discolouring of the solutions can be seen at 2 $mg\,mL^{-1}$ GNP concentrations due to haemolysis. We suspect there maybe cytotoxicity at such high concentrations possibly caused by the ethylene glycol units of the spacer molecule resulting in cell membrane damage;[62] however, at lower concentrations this is not seen. The inhibition power of **GNPs 2–6** can be seen in Table 2. The corresponding monomer **2SAc** (protected thiol form of the galactose conjugate **2** in free solution) was assigned a relative activity value of 1.

Table 2. Results from hemagglutination inhibition assays for PA-IL. nd = not determined, no inhibition observed at 2 $mg\,mL^{-1}$ or below. Errors are the variation in valency within the population of GNPs.

Ligand	Galactose valency	Galactose valency [%]	Inhibiting sugar conc. [μM]	Relative activity per ligand
2SAc	1		45.5	1
GNP-2	12	17	(12.5±1.0)	(4.0±0.3)
GNP-3	15	33	(1.02±0.07)	(45±1)
GNP-4	65	80	(0.66±0.01)	(69±1)
GNP-5	57	90	(0.40±0.01)	(114±2)
GNP-6	67	100	(0.45±0.01)	(101±2)
GNP-1	0	0	nd	nd
GNP-8	24 (Man)	25 (Man)	nd	nd

Even with low density presentations (**GNP-2**, galactose 17%), a subtle cluster glycoside effect can be observed for the ligands presented on the GNP scaffold. A significant improvement in inhibition power is observed for low valency **GNP-3** (galactose 33%), with minimum galactoside concentrations approaching 1 μM. This inhibition power (or cluster glycoside effect) is then amplified upon further increasing galactose presentation density, with minimum galactoside concentrations in the nM range. An activity factor over 100 times stronger was observed per galactose ligand for **GNP-5** (galactose 90%) and **GNP-6** (galactose 100%) with respect to **2SAc**. However, an increase in inhibition power between **GNP-4** and **GNP-5** indicates that GNP valency is less important than presentation density. This is again confirmed upon a reduction in inhibition power between **GNP-5** and **GNP-6**. This could be due to subtle alterations in ligand presentation and organisation at the GNP surface from 80 to 90 to 100% galactose presentations. For **GNP-6**, despite an increase in galactose valency, no further galactose ligands may be available for binding PA-IL units–the "effective valency" of a GNP with a high ligand presentation density maybe similar to the actual valency of a GNP with a lower presentation density. Therefore, **GNP-6** may in fact have the same inhibition power, per "effective ligand", which is then averaged over all galactosides on the GNP surface, available or not.

Binding kinetics by surface plasmon resonance: Surface plasmon resonance (SPR) was used to study the kinetics and quantify the interaction between the galactose-GNPs and PA-IL. 300 RUs of PA-IL were immobilised to a CM5 sensor chip (Biacore/GE, Uppsala, Sweden). Ethanolamine was immobilised to a second channel of the CM5 sensor chip to serve as a blank surface. A third channel was functionalised with 500 RUs of the lectin BC2L-A,[63] a mannose specific lectin, as a negative control for non-specific galactose–GNP interactions and a positive control for mannose–GNP activity. Solutions of **GNP-1–10** in HEPES buffer were flowed over the sensor chip with concentrations of 20 $\mu g\,mL^{-1}$ and serial dilutions thereof to 300 $ng\,mL^{-1}$. The galactose containing **GNP-2–6** showed significant binding to the PA-IL surface (see the Supporting Information, Figure 6S). A typical sensorgram for **GNP-6** can be seen in Figure 3. A one site binding model was applied in the BIA evaluation software (Uppsala, Sweden) to fit the association and dissociation of the GNPs to the PA-IL surface. A one site model was used as this gave the best fit and the lowest χ^2 value. The association (k_a) and dissociation (k_d) rate constants as well as the calculated association (K_a) and dissociation (K_d) constants are shown in Table 3. As expected, **GNP-1** and **GNP-7–10**, displaying glucose and mannose on their surface showed no binding to the PA-IL channel. The mannose-GNPs showed strong binding to the BC2L-A surface whilst the galactose-GNPs did not (data not shown). None of the GNPs tested showed binding to ethanolamine.

It can be seen from Table 3 that the trend in K_a is in agreement with the trend in inhibitory power from HIA, with large increases in K_a upon increasing galactose presentation density. By comparing the binding activity of **GNP-2** and **GNP-5**, there is over a 6000-fold difference between a galactose presentation density of 17 and 90%. However, as for the HIA experiments, there is a decrease in binding activity for the highest presentation density, **GNP-6**, despite an increase in GNP valency. The preference of PA-IL for larger presentation densities could be explained by a combination of structural preferences and statistical binding. As the presentation density increases, individual ligands may self-organise into semi-rigid clusters reducing entropic penalties for multivalent binding. The large increase in K_a observed for **GNP-5** is clearly related to a significant decrease

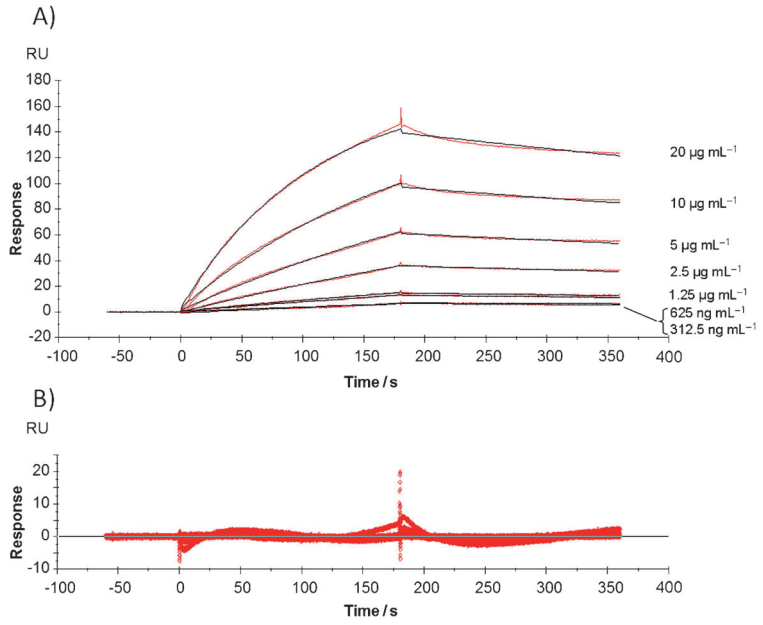

Figure 3. A) SPR sensorgram for solutions of **GNP-6** passing over a CM5 channel functionalised with 300 RUs of PA-IL. GNP serial dilutions of 20 μg mL^{-1} to 312.5 ng mL^{-1} were made. B) Plots showing deviations of data points from the fit (residuals) are also shown. Red points represent the data points, the black lines represent the theoretical fits.

Table 3. Affinity and dissociation rate constants and calculated K_a as measured for PA-IL by SPR. Data shown are based on single measurements.

GNP	k_a [10^3 M^{-1} s^{-1}]	k_d [10^{-6} s^{-1}]	K_a [10^9 M^{-1}]	K_d [nM]
GNP-2	16	291	0.05	20
GNP-3	69	249	0.28	3.6
GNP-4	69	41	1.67	0.6
GNP-5	25	0.08	306	0.003
GNP-6	25	783	0.03	33

in the macroscopic dissociation rate. This has been related to a decrease in entropic penalties of the ligand leaving the binding site.[64] At the same time, higher ligand densities will increase the probability of correct structural overlap of ligands and receptor binding sites as well as statistical rebinding. However, at the largest presentation, the restricted movement of the ligands at the GNP surface would indeed reduce entropic penalties, but would in turn exaggerate enthalpic penalties due to subtle incompatibilities in protein-receptor structural complementarity.

Binding thermodynamics by isothermal titration calorimetry: A further investigation of the thermodynamics of PA-IL-GNP binding was then carried out using isothermal titration microcalorimetry (ITC). HIA and SPR studies have demonstrated that presenting multivalent glycoclusters on a GNP platform results in significant affinity improvements for PA-IL binding. Due to the therapeutic importance of PA-IL regarding pathogen invasion, ITC was used to further characterise the interaction of PA-IL and galactose–GNPs. The thermograms and titration curves obtained for **2SAc** and GNP solutions can be seen in Figure 4.

Lectin concentrations are expressed as monomer concentration hence the single-site binding model was used to fit the data. The concentration of the nanoparticles was expressed as a concentration of galactose residues, confirmed by a modified phenol–sulfuric acid method.[61] The reaction stoichiometry (n) is defined as the number of monomeric galactose units per monomeric subunit of the lectin. It should be noted that the n value for monovalent **2SAc** relative to the lectin was fixed to the number of binding sites observed per monomer in the crystal structure ($n=1$).[65] K_a, K_d, thermodynamic parameters and binding stoichiometry for **2SAc** and GNPs tested are listed in Table 4 and shown in Figure 5. It was found that **GNP-4** and **GNP-5**, which have an 80 and 90% coverage of galactose residues, respectively, were insoluble in buffer solutions hence no ITC data is given. Injections of buffer solution into GNP solutions resulted in negligible heats of dilution. Injections of PA-IL into solutions of mannose-functionalised **GNP-8** (see the Supporting Information, Figure 7S) served as a reference for lectin dilution, which was subtracted from the galactose–GNP thermograms.

From the raw data, strong exothermic sigmoidal curves can be observed for the addition of PA-IL to the GNP solutions. The gradients of the sigmoid curves also give an indication of increased binding. Variations in galactose stoichiometry, n, also suggest varying ligand availabilities at different GNP presentation densities. The dissociation constant of 141 μM observed for **2SAc** is comparable to that previously observed for galactose monosaccharides and trisaccharides.[66] However, larger enthalpic and entropic contributions are observed for **2SAc**, most likely due to contributions from the linker molecule. From the dissociation constants observed for the GNP systems, there is a clear increase in PA-IL affinity even with a low presentation density on the GNP surface, as seen previously for HIA and SPR. The K_d of **GNP-2**, with a ligand presentation of 17%, was measured in the low micromolar range, with a binding potency factor, β (in which $\beta = K_{d,2SAc}/K_{d,GNP}$),[3] of 24. This improvement can be seen thermodynamically as a reduction in entropic penalties, despite a reduction in enthalpy. Upon increasing the ligand presentation density to 33%, for **GNP-3**, the dissociation constant falls to the mid-nanomolar range. The in-

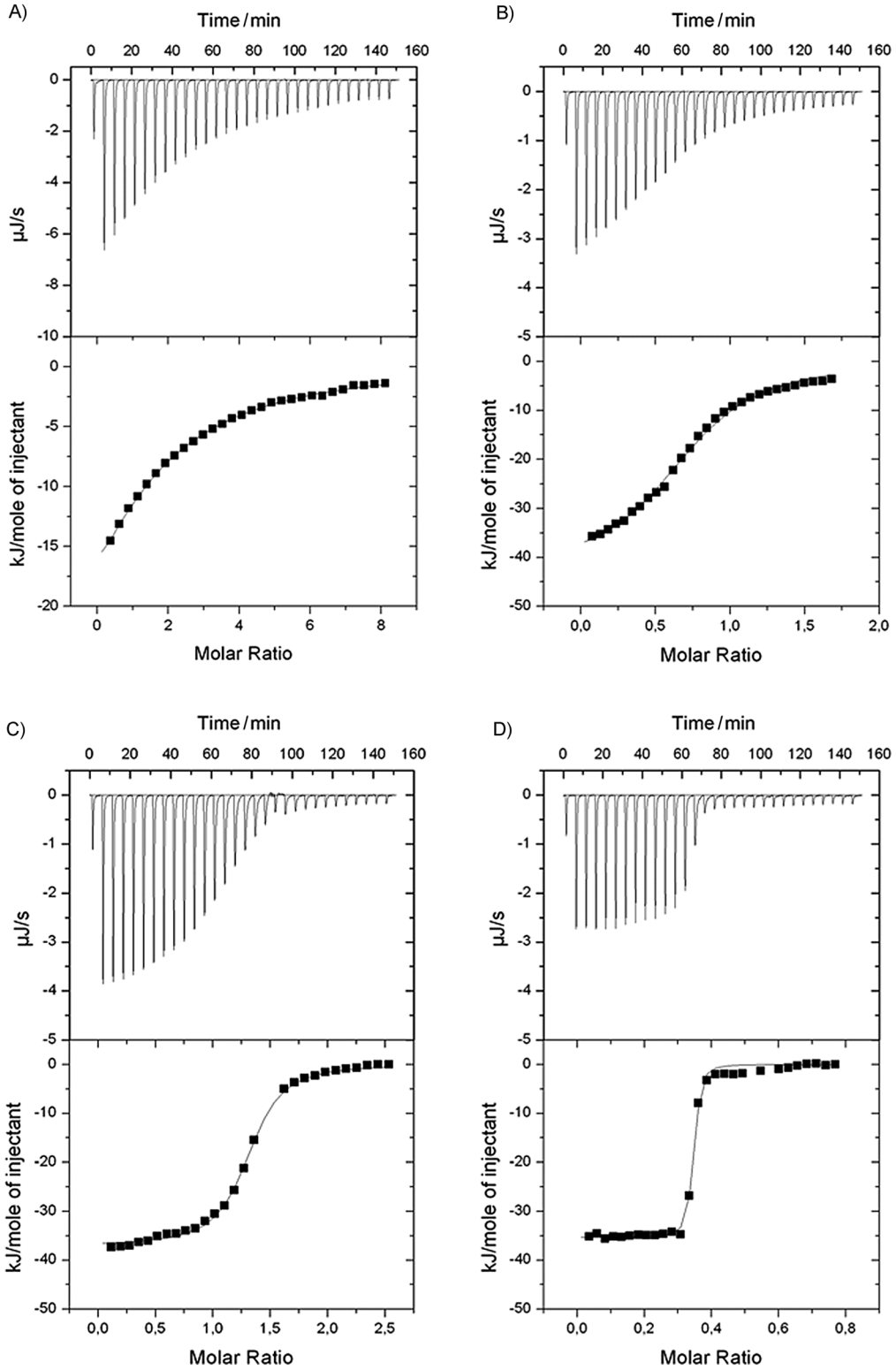

Figure 4. ITC profiles for A) the "standard" titration of PA-IL ([PA-IL_{mon}] = 0.047 mM in the cell) by injections of the galactose monomer, **2SAc** ([**2SAc**] = 1.7 mM in the syringe). The molar ratio here refers to the number of galactoside monomers per PA-IL binding site. B)–D) "reverse" titrations of the GNPs (in the cell) by PA-IL (in the syringe). Molar ratios here refer to the number of PA-IL binding sites per galactoside ligand. B) reverse titration of **GNP-2** (galactoside concentration in the cell, [**2**] = 0.048 mM) by injections of PA-IL ([PA-IL_{mon}] = 0.36 mM in the syringe), C) the reverse titration of **GNP-3** (galactoside concentration in the cell, [**2**] = 0.031 mM) by PA-IL ([PA-IL_{mon}] = 0.35 mM in the syringe) and D) the reverse titration of **GNP-6** (galactoside concentration in the cell, [**2**] = 0.07 mM) by PA-IL ([PA-IL_{mon}] = 0.24 mM in the syringe). Concentrations of the galactoside, **2**, are given as (monovalent) thiol concentrations. All experiments were carried out at 25 °C. Solid black squares represent the data points, the black lines represent the theoretical fits.

Table 4. Results of the interactions between PA-IL and galactose-functionalised GNPs, as found by ITC. Errors are the standard deviations over 2 or 3 experiments. β is the potency of binding with reference to the monomer **2SAc**. All stoichiometries refer to the number of galactosides per PA-IL binding site.

Ligand	K_a [10^6 M^{-1}]	K_d [μM]	n [stoichiometry]	ΔG [kJ mol^{-1}]	ΔH [kJ mol^{-1}]	$-T\Delta S$ [kJ mol^{-1}]	β
2SAc	(0.007±0.001)	141	1[a]	(−22.0±0.4)	(−65±3)	(43±3)	1
GNP-2	(0.17±0.03)	5.8	(1.2±0.2)	(−29.9±0.4)	(−37±7)	(6.7±6.7)	24
GNP-3	(1.3±0.8)	0.76	(0.76±0.04)	(−34±3)	(−54±9)	(20±12)	185
GNP-6	(20±2)	0.05	(2.1±0.6)	(−41.7±0.3)	(−18±5)	(−23±5)	2824

[a] Stoichiometry was fixed to 1 according to the crystal structure.

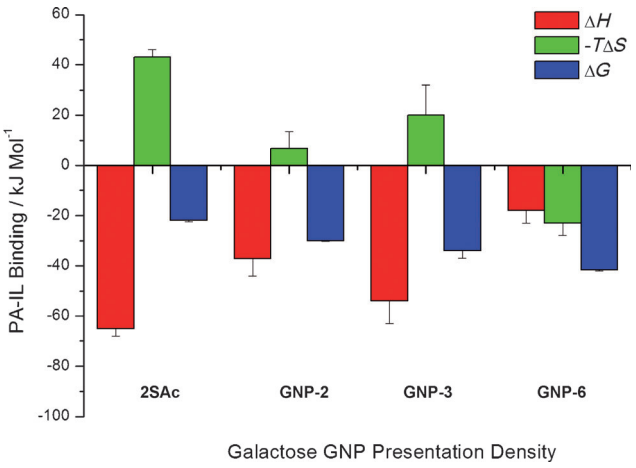

Figure 5. Graphs of ITC results for PA-IL. Thermodynamic parameters of the binding of PA-IL to galactose-functionalised GNPs; ΔG (blue), ΔH (red) and $-T\Delta S$ (green).

crease in PA-IL affinity in this case is dominated by enthalpic contributions. Further increasing the presentation density to 100% gives a K_d of 50 nM per galactose ligand, nearly a 3000-fold affinity enhancement, characterised by favourable entropic contributions. Although there is a clear reduction in enthalpy, this would be enthalpy averaged over all galactose residues. Given that $n=2$ for **GNP-6**, only half of the galactose residues are available for binding to PA-IL. The total observed change in enthalpy is subsequently averaged over all ligands, whether available to interact with a PA-IL binding site or not. From this we can infer that having an optimum ligand presentation density is important for increasing enthalpic contributions, yet, higher densities are necessary to have the same "effective valency" with less entropic penalties. Nevertheless, **GNP-6** is the highest affinity ligand identified for PA-IL to date.

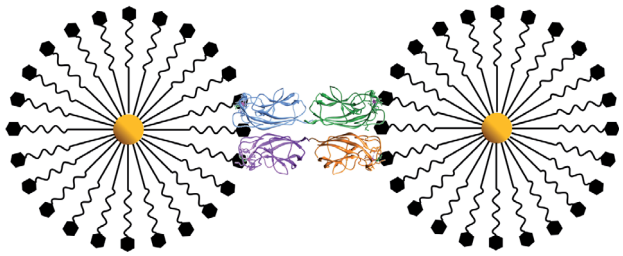

Figure 6. Schematic of the chelate complex formed between PA-IL and galactose-functionalised GNP. Diagram not to scale.

Considering the interaction at the molecular level, due to the architecture of the lectin (Figure 6), chelation of the four binding sites by ligands presented on the same GNP is unlikely. However, intermolecular interactions of one PA-IL tetramer with several different GNPs would be possible and may lead to aggregate structures, as seen by Sisu et al., and their study of LTBh with multivalent GM1 ligands,[67] particularly at sub-stoichiometric concentrations of PA-IL. As the experiment proceeds however and the PA-IL concentration increases, one would expect the formation of "chelate complexes", where two GNPs bind bivalently to opposite faces of the PA-IL tetramer (Figure 6, a more refined diagram can be found in the Supporting Information), as suggested previously by Cecioni et al.[33] and Otsuka et al.[27] In previous ITC studies of PA-IL with multivalent ligands this chelate complex is characterised by favourable enthalpic contributions and reduced entropic penalties.[68] As the PA-IL concentration approaches saturation of the galactose ligands, these chelate complexes would most likely dissociate to only one face of the PA-IL tetramer binding to a GNP. From both a structural complementarity and statistical binding point of view, bidentate binding of PA-IL by ligands presented on an AuNP platform will be increasingly favourable with higher presentation densities. From a low density presentation to a moderate density, a greater probability of correct ligand-binding site overlap will occur allowing for enthalpic enhancement. Upon further increasing to high density presentations, the pre-organised ligands at the GNP surface will induce favourable entropic contributions whilst small structural incompatibilities will be exaggerated in the form of enthalpic penalties. Nevertheless, the effective concentrations of ligand-binding sites will increase the probability of statistical rebinding.

Comparison of HIA, SPR and ITC: To gain a general insight into biochemical interactions, a combination of analytical techniques is required depending on the nature and properties of the event to be observed. We have shown that the different bioanalytical assays used in this study are in agreement with the strong affinity of galactose ligands presented on a gold nanoparticle. In all experiments the same general trend has been observed; ligands presented on a gold nanoparticle exhibit a significant increase in avidity for their lectin receptors compared to the ligands in free solution. Low ligand presentation densities give rise to a significant increase in ligand affinity. Upon increasing ligand presentation density, ligand activity increases further still. HIA and SPR exhibited similar behaviour regarding inhibitory power, interaction kinetics and presentation density, with an increase in ligand activity with presentation density followed by a reduction in ligand activity at 100% ligand presenta-

tion. ITC has shown that **GNP-6**, which shows a 100% ligand presentation density, exhibits a 2800-fold increase in ligand activity compared with the galactose ligand in free solution. With a K_d of 50 nM, this is the most effective PA-IL ligand to date.

Although the techniques used are in broad agreement, they do exhibit certain differences and discrepancies. The reason for such differences is most certainly due to the fact that the different techniques are measuring the same binding event but through different phenomena. HIA, for example, is concerned with homogeneous phase aggregation behaviour, whereas ITC measures homogeneous phase binding in solution and SPR heterogeneous binding and dissociation in which one binding partner is immobilised to a surface. On one hand, immobilising PA-IL to a SPR chip surface may reduce the effects of translational and rotational entropy upon ligand binding. On the other hand when in free solution, as in the case of an ITC experiment, these entropy effects maybe further exaggerated during ligand binding when compared with the natural state of the lectin.

The increase in ligand activity at GNPs can be explained by a combination of structural complementarities and effective concentration theories regarding multivalence and cluster glycoside effects. Increasing presentation density may lead to correct ligand—binding-site overlap whilst also preorganising ligand presentation at the GNP surface thus decreasing entropic penalties and increasing the probability of statistical rebinding.

Conclusion

In summary, we have reported the synthesis and characterisation of galactose-functionalised GNPs. These GNPs exhibit several ligand presentation densities ranging from 17–100% (with respect to an inert glucose conjugate). These biofunctionalised gold nanoparticles can be used as multivalent platforms for presenting carbohydrate molecules, as well as for observing the effect of valency, presentation density, and ligand behaviour on their recognition by protein receptors. The increase in lectin affinity for nanoparticle-based carbohydrate ligands has been observed both qualitatively by hemagglutination inhibition assays, as well as quantitatively using surface plasmon resonance, and the first use of isothermal titration microcalorimetry for nanoparticle-scaffolded carbohydrate ligand systems. For the PA-IL lectin, from *Pseudomonas aeruginosa*, we have shown that even low galactoside presentation densities on the GNPs can increase lectin recognition. At the highest galactose presentation density, almost a 3000-fold increase in ligand activity was observed here.

We have confirmed that glyconanoparticle technology offers a tuneable synthesis for improved ligand presentation. For the PA-IL lectin, we have demonstrated that the GNP multivalent ligand system provides the most efficient binding partner to date with a K_d of 50 nM–another example of their potential application as potent anti-adhesives for the prevention of pathogen invasion.[69,70] The platform has the potential to be simultaneously tailored with several different ligands. In particular, a GNP functionalised with both galactose and fucose could prove an interesting multifunctional inhibitor for both PA-IL and PA-IIL lectins as a combined approach to prevent infection by *Pseudomonas aeruginosa*.[71] Furthermore, different biologically or diagnostically important molecules (immunogenic peptides or other antigens, fluorescent markers, etc.) can be grafted to the GNP surface, allowing the preparation of multifunctional structures for use as carbohydrate-based inhibitors, drug delivery agents and diagnostics. Concurrently with applications research, further experimental, computational or crystallographic studies on AuNP and GNP structure and formation would provide more detailed, fundamental information regarding ligand presentation and behaviour. This in turn would allow for a fuller interpretation and exploitation of the multivalence/cluster glycoside effect at the molecular level.

Experimental Section

General procedures: All starting materials were purchased from Sigma–Aldrich and used without further purification with the exception of tetrachloroauric acid monohydrate which was purchased from Strem Chemicals and used without further purification. Reactions were monitored by thin-layer chromatography (TLC) on Silica Gel 60 F_{254} aluminium-backed sheets (Merck) with visualisation under UV (254 nm) and/or by staining with *para*-anisaldehyde solution (anisaldehyde (25 mL), H_2SO_4 (25 mL), EtOH (450 mL) and CH_3COOH (1 mL)), phosphomolybdic acid solution (phosphomolybdic acid (1.3 g), cerium (IV) sulfate monohydrate (1 g), concentrated sulfuric acid (6 mL) water (made up to 100 mL)) or Potassium permanganate solution ($KMnO_4$ (2.5 g), K_2CO_3 (20 g), NaOH (10%), H_2O (200 mL)) as stated in the protocol, followed by heating at over 200 °C. Size-exclusion chromatography was performed on Sephadex LH-20 (Sigma). Flash column chromatography (FCC) was carried out on Silica Gel 60 (0.063–0.2 mm; E. Merck). All dialyses were carried out using SnakeSkin pleated dialysis membranes (Pierce, 3500 MWCO). UV/Vis spectra were measured with Varian Cary 50 Bio UV/Vis spectrometer. Infrared (IR) spectra were recorded from 4000 to 400 cm^{-1} with a PerkinElmer FT-IR spectrometer. Samples were pressed into KBr pellets. ^1H and ^{13}C NMR spectra were acquired on Bruker AVANCE 400 MHz and Bruker AC 300 MHz spectrometers. Chemical shifts (δ) are given in ppm relative to the residual signal of the solvent used. Coupling constants (J) are reported in Hz. Splitting patterns are described by using the following abbreviations: br, broad; s, singlet; d, doublet; t, triplet; m, multiplet. Mass spectra were recorded on a ZQ Waters Electrospray LC/MS. For transmission electron microscopy (TEM) examinations, a single drop (10 μL) of an aqueous solution (ca. 0.1 $mg\,mL^{-1}$ in Milli-Q water) of the gold glyconanoparticles (GNPs) was placed on carbon-coated 200 μm mesh copper grids. The grid was covered and left to dry in air for several hours at room temperature. TEM analysis was performed with a JEOL 3010 microscope operating at 300 kV to a magnification of 500 000. The photographs were taken on Kodak SO163 films which were then digitalised using a Kodak Mega Plus camera. The diameters of 350–3000 particles were measured for each GNP, using the Scandium 5.0 software (Soft Imaging Systems). The average diameters and numbers of gold atoms of the GNPs were deduced as described in a previous study.[57] Laboratory distilled water was further purified using a Milli-Q water purification system. For clarity, the neoglycoconjugates are all named and depicted as disulfides.

Small-angle X-ray scattering: Aqueous nanoparticle solutions of 2 $mg\,mL^{-1}$ were prepared and centrifuged for 2×5 min at 13 000 rpm.

SAXS was carried out at the ID02 high brilliance and ID13 microfocus beamlines of the European Synchrotron Radiation Facililty (ESRF) using a monochromatic beam of $\lambda = 1.0597$ Å ($E = 11.7$ keV) and $\lambda = 1$ Å ($E = 12.39$ keV), respectively. Sample–detector distances of 1.5 m and 0.787 m were used giving q ranges of 0.06–4 and 0.2–3 nm^{-1} respectively. SAXS patterns were recorded by a 16 bit readout FReLoN charge coupled device (CCD) detector with 2048×2048 pixels of 51×51 μm^2 binned to 512×512 pixels. Nanoparticle and water solutions were studied in a 1.7 mm diameter flow-through cell or 200 μm glass capillary. SAXS patterns were obtained after correction and background subtraction. Between 5 and 10 SAXS patterns were corrected and averaged for fitting. Data analysis was carried out using the *SAXSutilities* package (www.sztucki.de/SAXSutilities).[72] A core-shell model from this package was used to fit the SAXS patterns. Core radii and polydispersity were set to those taken from TEM. Shell radii were extracted from the fits.

Recombinant proteins: The lectin PA-IL from *Pseudomonas aeruginosa*, was expressed and purified in recombinant form from *Escherichia coli* as documented previously.[65]

Monosaccharide analysis: Monosaccharide analysis was carried out using a variation of the Phenol-sulfuric acid method documented by Saha et al.[61] Calibration curves were made using solutions of varying concentrations (31.3 ng mL^{-1} to 1 mg mL^{-1}) of Me-β-D-Glucopyranoside and Me-β-D-Galactopyranoside corresponding to GNP coverage densities as determined by NMR, TEM and elemental analysis. To a GNP solution (50 μL), 5% (v/v) Phenol (aq.) solution (50 μL) was added and mixed. H_2SO_4 (250 μL) was added, the mixture was vortexed, and allowed to stand for 30 mins at room temperature. Readings were taken at 490 nm against a blank prepared substituting buffer solution for the GNP solution. Serial dilutions of GNP solutions were also used to confirm carbohydrate concentration and to ensure readings were taken within the workable range of the spectrophotometer. A Varian Cary 50 Bio spectrophotometer was used for the absorbance measurements at 490 nm.

Hemagglutination inhibition assay: Rabbit erythrocytes were bought from Biomerieux and used without further washing. The erythrocytes were diluted to a 2% solution in NaCl (150 mM). Lectin solutions (1 mg mL^{-1}) were prepared in Tris/HCl as for the calorimetry studies. The Hemagglutination unit (HU) was first obtained by the addition of 25 μL of the 2% erythrocyte solution to 25 μL aliquots of sequential lectin dilutions. The mixture was incubated at 37 °C for 30 mins followed by incubation at RT for 30 mins. The HU was taken as the minimum lectin concentration required to prevent hemagglutination. For the following lectin-inhibition assays, lectin concentrations of four times that of the hemagglutination unit were used. For PA-IL, this concentration was found to be 5 μg mL^{-1}. Subsequent assays were then carried out by the addition of 50 μL lectin solution (at the required concentration) to 50 μL of sequential dilutions of GNPs, monomer molecules and controls. These solutions were then incubated at 37 °C for 30 mins followed by 30 mins at RT. After which, 50 μL of 2% erythrocyte solution was added followed by a further 30 mins incubation at 37 °C and 30 mins at RT. The minimum inhibitory concentration for each GNP molecule was recorded.

Surface plasmon resonance assays: All SPR experiments were carried out on a Biacore T100 instrument. CM5 sensor chips (Biacore/GE, Uppsala, Sweden) were equilibrated with HBS (HEPES-buffered saline: 10 mM HEPES and 150 mM NaCl, pH 7.4) containing 0.005% (v/v) Tween 20 at 25 °C with a flow rate of 20 μL min^{-1}. Following equilibration, the chips were activated with two 7 min pulses of a 1:1 mixture (v/v) of 0.1 M *N*-hydroxy-succinimide and 0.1 M *N*-ethyl-*N*′-(dimethylaminopropyl)carbodiimide, at 25 °C and flow rate of 5 μL min^{-1}. Ethanolamine hydrochloride was immobilised on channel one through an injection of 7 min (1.0 M, pH 8.5; ≈80 RU) to measure the level of non-specific binding and to serve as a blank for mathematical data treatment. PA-IL was immobilised to Channel 3 through an injection of 41 mins (100 μg mL^{-1}, Sodium Acetate buffer, pH 4.5; ≈300 RU). Remaining *N*-hydroxy succinimide esters were blocked by a 7 min pulse of 1.0 Ethanolamine hydrochloride, pH 8.5.

Affinity measurements: For the surface functionalised with PA-IL, GNP solutions (20 μg mL^{-1}, and dilutions thereof to 300 ng mL^{-1}) in HEPES buffer were flowed across the sensor chip surface surfaces for 3 mins at a flow rate of 20 μL min^{-1}, and were allowed to dissociate for 3 mins. The surface was regenerated with 3×3 min pulses of 100 mM Me-α-D-galactose. Surface regeneration was again confirmed by a repeat injection of a GNP solution at 1.25 μg μL^{-1} at the end of the concentration series. Binding was measured as RU (resonance units) over time. Affinity (k_a) and dissociation constant (k_d) rates were calculated using the BIA evaluation software 1.1 (Biacore). Curves were fitted to a single 1:1 binding model, which gave the best fit as judged by the lowest χ^2 value and the best distribution of residuals. Association constants (K_a) were calculated from the equation: $K_a = 1/K_d = k_a/k_d$

Microcalorimetry: Titration calorimetry experiments were performed using a Microcal VP-ITC microcalorimeter. Titrations were carried out in 0.1 M Tris/HCl buffer (pH 7.5) containing 3 μM $CaCl_2$, at 25 °C. 30–40 aliquots of 7.5–10 μL of lectin solutions with concentrations of 0.23 mM to 1 mM, were added at 5 min intervals to the GNP solution present in the calorimeter cell. In the titrations, the GNP concentration varied from 0.46 mg mL^{-1} to 1.12 mg mL^{-1} PA-IL, giving a saccharide concentration of 0.031 mM to 0.076 mM as found by the phenol-sulfuric acid method mentioned above. The corresponding monomer molecule, **2SAc**, was also injected into solutions of PA-IL. **2SAc** concentrations were 1.7 mM and PA-IL concentrations 0.05 mM. The temperature of the cell was controlled to (25 ± 0.1) °C. Control experiments performed by injection of buffer into the GNP solution yielded insignificant heats of dilution. Injections of lectin into control (mannose functionalised) GNPs yielded heats of dilution, which were subtracted from experimental data during the data processing phase. Integrated heat effects were analysed by nonlinear regression using a one-site binding model (Origin 7.0, OriginLab Corp.). Fitted data yielded association constants (K_a) and the enthalpy of binding (ΔH). Other thermodynamic parameters, i.e.; changes in free energy, ΔG, and entropy, ΔS, were calculated from the equation: $\Delta G = \Delta H - T\Delta S = -RT\ln K_a$, in which T is the absolute temperature and $R = 8.314$ J mol^{-1} K^{-1}. Two to three independent titrations were performed for each lectin–GNP combination.

Acknowledgements

The authors wish to thank the GlycoGold Research Training Network, a part of the sixth research framework of the European Union, contract number MRTN-CT-2004–005645, for financial support. Financial support from the CNRS and ESRF are also acknowledged. We thank also the Spanish Ministry of Science and Innovation (MICINN, grant CTQ2008–04638) and the Department of Industry of the Basque Country (Etortek 2009). This project was also supported by COST action CM1102. Dr Bertrand Blanchard is greatly appreciated for help with lectin production; Catherine Gautier's help with ITC is also appreciated. The SPR experiments were ran thanks to access to a Biacore T100 at the Plateforme Nanobio-Grenoble. We would also like to thank Isabelle Paintrand (CERMAV-CNRS) and Dr Patricia Donnadieu (SIMAP, INP, Grenoble) for the TEM photographs. SAXS experiments and analysis were carried out with the help of Dr. Michael Sztucki and Dr. Emanuela Di Cola (ESRF, Grenoble). Professors Monica Palcic and Johannis Kamerling are also thanked for their helpful discussions.

[1] A. Varki, R. D. Cummings, J. D. Esko, H. H. Freeze, P. Stanley, C. R. Bertozzi, G. W. Hart, M. E. Etzler, *Essentials of Glycobiology, 2nd ed.*, Cold Spring Harbour, New York, **2009**.
[2] H. Lis, N. Sharon, *Chem. Rev.* **1998**, *98*, 637–674.
[3] M. Mammen, S. K. Choi, G. M. Whitesides, *Angew. Chem.* **1998**, *110*, 2908–2953; *Angew. Chem. Int. Ed.* **1998**, *37*, 2754–2794.
[4] Y. C. Lee, R. T. Lee, *Acc. Chem. Res.* **1995**, *28*, 321–327.
[5] L. L. Kiessling, J. E. Gestwicki, L. E. Strong, *Curr. Opin. Chem. Biol.* **2000**, *4*, 696–703.
[6] J. J. Lundquist, E. J. Toone, *Chem. Rev.* **2002**, *102*, 555–578.
[7] R. H. Kramer, J. W. Karpen, *Nature* **1998**, *395*, 710–713.

[8] J. M. Gargano, T. Ngo, J. Y. Kim, D. W. Acheson, W. J. Lees, *J. Am. Chem. Soc.* **2001**, *123*, 12909–12910.
[9] T. A. Shewmake, F. J. Solis, R. J. Gillies, M. R. Caplan, *Biomacromolecules* **2008**, *9*, 3057–3064.
[10] R. S. Kane, *Langmuir* **2010**, *26*, 8636–8640.
[11] V. M. Krishnamurthy, V. Semetey, P. J. Bracher, N. Shen, G. M. Whitesides, *J. Am. Chem. Soc.* **2007**, *129*, 1312–1320.
[12] M. Reynolds, S. Perez, *C. R. Chim.* **2011**, *14*, 74–95.
[13] I. J. Krauss, J. G. Joyce, A. C. Finnefrock, H. C. Song, V. Y. Dudkin, X. Geng, J. D. Warren, M. Chastain, J. W. Shiver, S. J. Danishefsky, *J. Am. Chem. Soc.* **2007**, *129*, 11042–11044.
[14] O. Renaudet, *Mini-Rev. Org. Chem.* **2008**, *5*, 274–286.
[15] B. Benaissa-Trouw, D. J. Lefeber, J. P. Kamerling, J. F. Vliegenthart, K. Kraaijeveld, H. Snippe, *Infect. Immun.* **2001**, *69*, 4698–4701.
[16] P. M. Rendle, A. Seger, J. Rodrigues, N. J. Oldham, R. R. Bott, J. B. Jones, M. M. Cowan, B. G. Davis, *J. Am. Chem. Soc.* **2004**, *126*, 4750–4751.
[17] T. K. Dam, H. J. Gabius, S. Andre, H. Kaltner, M. Lensch, C. F. Brewer, *Biochemistry* **2005**, *44*, 12564–12571.
[18] K. J. Doores, D. P. Gamblin, B. G. Davis, *Chem. Eur. J.* **2006**, *12*, 656–665.
[19] H. Nagai, A. Onoda, T. Matsuo, T. Hayashi, *Supramol. Chem.* **2010**, *22*, 57–64.
[20] M. J. Cloninger, *Curr. Opin. Chem. Biol.* **2002**, *6*, 742–748.
[21] R. Roy, M. G. Baek, *Rev. Mol. Biotechnol.* **2002**, *90*, 291–309.
[22] W. B. Turnbull, J. F. Stoddart, *Rev. Mol. Biotechnol.* **2002**, *90*, 231–255.
[23] C. D. Heidecke, T. K. Lindhorst, *Chem. Eur. J.* **2007**, *13*, 9056–9067.
[24] S. K. Wang, P. H. Liang, R. D. Astronomo, T. L. Hsu, S. L. Hsieh, D. R. Burton, C. H. Wong, *Proc. Natl. Acad. Sci. USA* **2008**, *105*, 3690–3695.
[25] R. Narain, S. P. Armes, *Biomacromolecules* **2003**, *4*, 1746–1758.
[26] L. Bes, S. Angot, A. Limer, D. M. Haddleton, *Macromolecules* **2003**, *36*, 2493–2499.
[27] I. Otsuka, B. Blanchard, R. Borsali, A. Imberty, T. Kakuchi, *ChemBioChem* **2010**, *11*, 2399–2408.
[28] D. Cade, E. Ramus, M. Rinaudo, R. Auzely-Velty, T. Delair, T. Hamaide, *Biomacromolecules* **2004**, *5*, 922–927.
[29] J. E. Gestwicki, L. E. Strong, S. L. Borchardt, C. W. Cairo, A. M. Schnoes, L. L. Kiessling, *Bioorg. Med. Chem.* **2001**, *9*, 2387–2393.
[30] J. F. Nierengarten, J. Iehl, V. Oerthel, M. Holler, B. M. Illescas, A. Munoz, N. Martin, J. Rojo, M. Sanchez-Navarro, S. Cecioni, S. Vidal, K. Buffet, M. Durka, S. P. Vincent, *Chem. Commun.* **2010**, *46*, 3860–3862.
[31] S. Cecioni, V. Oerthel, J. Iehl, M. Holler, D. Goyard, J. P. Praly, A. Imberty, J. F. Nierengarten, S. Vidal, *Chem. Eur. J.* **2011**, *17*, 3252–3261.
[32] L. Baldini, A. Casnati, F. Sansone, R. Ungaro, *Chem. Soc. Rev.* **2007**, *36*, 254–266.
[33] S. Cecioni, R. Lalor, B. Blanchard, J. P. Praly, A. Imberty, S. E. Matthews, S. Vidal, *Chem. Eur. J.* **2009**, *15*, 13232–13240.
[34] A. Dondoni, A. Marra, *Chem. Rev.* **2010**, *110*, 4949–4977.
[35] S. Cecioni, S. Faure, U. Darbost, I. Bonnamour, H. Parrot-Lopez, O. Roy, C. Taillefumier, M. Wimmerova, J. P. Praly, A. Imberty, S. Vidal, *Chem. Eur. J.* **2011**, *17*, 2146–2159.
[36] A. Robinson, J. M. Fang, P. T. Chou, K. W. Liao, R. M. Chu, S. J. Lee, *ChemBioChem* **2005**, *6*, 1899–1905.
[37] J. D. M. de La Fuente, S. Penades, *Tetrahedron: Asymmetr.* **2005**, *16*, 387–391.
[38] K. Niikura, S. Sekiguchi, T. Nishio, T. Masuda, H. Akita, Y. Matsuo, K. Kogure, H. Harashima, K. Ijiro, *ChemBioChem* **2008**, *9*, 2623–2627.
[39] R. Kikkeri, B. Lepenies, A. Adibekian, P. Laurino, P. H. Seeberger, *J. Am. Chem. Soc.* **2009**, *131*, 2110–2112.
[40] Y. Yang, M. Yu, T. T. Yan, Z. H. Zhao, Y. L. Sha, Z. J. Li, *Bioorg. Med. Chem.* **2010**, *18*, 5234–5240.
[41] J. M. de La Fuente, A. G. Barrientos, T. C. Rojas, J. Rojo, J. Canada, A. Fernandez, S. Penadés, *Angew. Chem.* **2001**, *113*, 2317–2321; *Angew. Chem. Int. Ed.* **2001**, *40*, 2257–2261.
[42] L. Sihelníková, I. Tvaroska, *Chem. Pap.* **2007**, *61*, 237–255.
[43] M. Marradi, M. Martin-Lomas, S. Penadés, *Adv. Carbohydr. Chem. Biochem.* **2010**, *64*, 211–290.
[44] I. Garcia, J. Gallo, M. Marradi, S. Penadés, in *Engineered Carbohydrate-Based Materials for Biomedical Applications: Polymers, Surfaces, Dendrimers, Nanoparticles and Hydrogels* (Ed.: R. Narain), Wiley, Hoboken, New Jersey, **2011,** pp. 213–259.
[45] P. H. Weigel, R. L. Schnaar, M. S. Kuhlenschmidt, E. Schmell, R. T. Lee, Y. C. Lee, S. Roseman, *J. Biol. Chem.* **1979**, *254*, 10830–10838.
[46] B. T. Houseman, M. Mrksich, *Angew. Chem.* **1999**, *111*, 876–880; *Angew. Chem. Int. Ed.* **1999**, *38*, 782–785.
[47] C. W. Cairo, J. E. Gestwicki, M. Kanai, L. L. Kiessling, *J. Am. Chem. Soc.* **2002**, *124*, 1615–1619.
[48] E. K. Woller, E. D. Walter, J. R. Morgan, D. J. Singel, M. J. Cloninger, *J. Am. Chem. Soc.* **2003**, *125*, 8820–8826.
[49] S. Takae, Y. Akiyama, H. Otsuka, T. Nakamura, Y. Nagasaki, K. Kataoka, *Biomacromolecules* **2005**, *6*, 818–824.
[50] A. G. Barrientos, J. M. Fuente, M. Jimenez, D. Solis, F. J. Canada, M. Martin-Lomas, S. Penadés, *Carbohydr. Res.* **2009**, *344*, 1474–1478.
[51] E. Boisselier, D. Astruc, *Chem. Soc. Rev.* **2009**, *38*, 1759–1782.
[52] P. Crespo, R. Litrán, T. C. Rojas, M. Multigner, J. M. de La Fuente, J. C. Sánchez-López, M. A. García, A. Hernando, S. Penadés, A. Fernández, *Phys. Rev. Lett.* **2004**, *93*, 087204.
[53] J. Glick, N. Garber, *J. Gen. Microbiol.* **1983**, *129*, 3085–3090.
[54] J. R. Govan, V. Deretic, *Microbiol. Rev.* **1996**, *60*, 539–574.
[55] A. Imberty, M. Wimmerova, E. P. Mitchell, N. Gilboa-Garber, *Microbes Infect.* **2004**, *6*, 221–228.
[56] O. Martínez-Ávila, K. Hijazi, M. Marradi, C. Clavel, C. Campion, C. Kelly, S. Penadés, *Chem. Eur. J.* **2009**, *15*, 9874–9888.
[57] M. J. Hostetler, J. E. Wingate, C.-J. Zhong, J. E. Harris, R. W. Vachet, M. R. Clark, J. D. Londono, S. J. Green, J. J. Stokes, G. D. Wignall, G. L. Glish, M. D. Porter, N. D. Evans, R. W. Murray, *Langmuir* **1998**, *14*, 17–30.
[58] A. G. Barrientos, J. M. de La Fuente, T. C. Rojas, A. Fernandez, S. Penadés, *Chem. Eur. J.* **2003**, *9*, 1909–1921.
[59] R. Ojeda, J. L. de Paz, A. G. Barrientos, M. Martin-Lomas, S. Penadés, *Carbohydr. Res.* **2007**, *342*, 448–459.
[60] N. R. Jana, L. A. Gearheart, S. O. Obare, C. J. Johnson, K. J. Edler, S. Mann, C. J. Murphy, *J. Mater. Chem.* **2002**, *12*, 2909–2912.
[61] S. K. Saha, C. F. Brewer, *Carbohydr. Res.* **1994**, *254*, 157–167.
[62] A. M. Blow, G. M. Botham, D. Fisher, A. H. Goodall, C. P. Tilcock, J. A. Lucy, *FEBS Lett.* **1978**, *94*, 305–310.
[63] E. Lameignere, L. Malinovska, M. Slavikova, E. Duchaud, E. P. Mitchell, A. Varrot, O. Sedo, A. Imberty, M. Wimmerova, *Biochem. J.* **2008**, *411*, 307–318.
[64] I. Papp, C. Sieben, A. L. Sisson, J. Kostka, C. Bottcher, K. Ludwig, A. Herrmann, R. Haag, *ChemBioChem* **2011**, *12*, 887–895.
[65] G. Cioci, E. P. Mitchell, C. Gautier, M. Wimmerova, D. Sudakevitz, S. Pérez, N. Gilboa-Garber, A. Imberty, *FEBS Lett.* **2003**, *555*, 297–301.
[66] B. Blanchard, A. Nurisso, E. Hollville, C. Tetaud, J. Wiels, M. Pokorna, M. Wimmerova, A. Varrot, A. Imberty, *J. Mol. Biol.* **2008**, *383*, 837–853.
[67] C. Sisu, A. J. Baron, H. M. Branderhorst, S. D. Connell, C. A. Weijers, R. de Vries, E. D. Hayes, A. V. Pukin, M. Gilbert, R. J. Pieters, H. Zuilhof, G. M. Visser, W. B. Turnbull, *ChemBioChem* **2009**, *10*, 329–337.
[68] T. K. Dam, C. F. Brewer, *Chem. Rev.* **2002**, *102*, 387–429.
[69] J. Rojo, V. Diaz, J. M. de La Fuente, I. Segura, A. G. Barrientos, H. H. Riese, A. Bernad, S. Penadés, *ChemBioChem* **2004**, *5*, 291–297.
[70] O. Martínez-Ávila, L. M. Bedoya, M. Marradi, C. Clavel, J. Alcami, S. Penadés, *ChemBioChem* **2009**, *10*, 1806–1809.
[71] I. Deguise, D. Lagnoux, R. Roy, *New J. Chem.* **2007**, *31*, 1321–1331.
[72] M. Sztucki, T. Narayanan, *J. Appl. Crystallogr.* **2007**, *40*, S459-S462.

Received: July 1, 2011
Published online: February 23, 2012

